Check for updates

Fluoranthene dyes for the detection of water content in methanol†

Yu-Chen Liu,‡[a] Guo-Dan Lu,‡[a] Jia-Hui Zhou,[a] Jie-Wei Rong,[b] Hui-Yan Liu [ID] *[a] and Hai-Ying Wang [ID] *[a]

Three novel fluoranthene dyes were obtained by cycloaddition reactions using acrylonitrile and dialkyl acetylenedicarboxylates. Their fluorescence properties in different polar–organic solvents were investigated systematically. Meanwhile, spectral changes induced by the addition of water in methanol were observed, indicating that these fluoranthenes dyes can be efficiently used to detect the water content in methanol as probes. Significantly, the practical test measurements for the water contents in methanol illustrated the measured results with the three fluorescent probes were basically consistent with the water content added artificially. This demonstrated the potential of these fluoranthene dyes as probes in measuring the water content in methanol.

Introduction

Water is the most common impurity in many industrial and chemical processes involving organic solvents. The detection and quantification of small amounts of water are of great significance in several fields of chemistry and industry.[1] For example, in chemistry, particularly in organometallic chemistry, the presence of water will lead to the quenching of the reactive organometallic compounds, inhibiting the reaction or lowering the yields, and furthermore due to the high reactivity of the aforementioned organometallic reagents, the presence of water can, under some circumstances, lead to catastrophic failures, such as fires and explosions. In addition, an industrial process where the presence of water plays a crucial yet detrimental role is petroleum based fuels. The presence of water will cause a drop in an engine's performance, but more importantly, when the temperature is low enough, emulsification and phase separation may occur, causing clogged fuel ducts, leading to engine damage and failure.[2] Therefore, various methods and techniques have been developed for the determination of water in a wide variety of organic solvents. Karl Fisher titration is the most common approach to the quantitative measurement of water in organic solvents.[3–6] Gas chromatography (GC) or liquid chromatography (LC) methods have been suggested for the detection of water.[7,8] Moreover, spectrophotometry and chemiluminescence have been combined with flow-injection analysis (FIA) for the detection of water.[9] Although these methods have been modified and improve,[10–12] some disadvantages such as slow reaction rate, requirement of personal skill of the analyst, and interference from other common co-existing species limit the application of the method. More recently, colorimetric or fluorescence methods are more convenient than standard instrumental methods for routine laboratory activities. Numerous probes have been designed based on a variety of dyes and fluorophores. In fact, fluorescent sensors for the sensitive sensing of the water content in organic solvents have been successfully designed using various fluorophores of 1,8-naphthalimide,[13–15] flavone derivatives,[16] 8-hydroxyquinolines,[17] 2,3-biphenyl quinoxaline 6-amine,[18] thioxanthone fluorophores,[19,20] poly(*m*-aminobenzoic acid)[11,21] and acridine orange-based optical fiber.[22–24] However, comparatively very little attention has been devoted to the interesting photophysical and optical properties of highly fluorescent organic dyes, fluoranthene derivatives.[25–30]

Fluoranthene is a very attractive fluorophore with a pentagon and three hexagons. The rigid planarized biphenyl structure of the fluoranthene unit leads to a wide band gap with blue emission and also provides high photoluminescence quantum yield, thermal and electrochemical stability. These properties make fluoranthene an interesting material for polymer electrolyte membrane fuel cells, blue-emitting OLEDs and chemosensors.[31–34] Moreover, fluoranthenes can be fluorinated, which is a common strategy to improve dye photostability for imaging applications.[35] Synthesis and derivatization of fluoranthenes have received much attention in the recent years. Diels–Alder reaction and transition metal-catalyzed reactions are the most commonly used methods for their synthesis.[36–38]

[a]*School of Chemistry & Materials Science, Jiangsu Normal University, Jiangsu Key Laboratory of Green Synthetic Chemistry for Functional Materials, Xuzhou 221116, P. R. China. E-mail: wanghy@jsnu.edu.cn; liuhuiyan72@163.com*

[b]*School of Chemistry and Materials Engineering, Huaian Normal University, Huaian, 232038, P. R. China*

† Electronic supplementary information (ESI) available: Experimental procedures, spectral data for all new compounds. CCDC 2093383. For ESI and crystallographic data in CIF or other electronic format see DOI: 10.1039/d1ra08392a

‡ Yu-Chen Liu and Guo-Dan Lu contributed equally.

Our research group is involved in developing new small molecule organic fluorescent dyes for their potential applications in applied sciences.[39–43] In this paper, we report a novel, simple and effective method for the synthesis of fluoranthene dyes and their fluorescence properties as fluorescent sensor for determing the water content in common organic solvents such as DMF, acetone, THF, chloroform, CH_2Cl_2, ethyl acetate, and methanol. The novel fluoranthene dyes were prepared by cycloaddition reactions using acrylonitrile and dialkyl acetylenedicarboxylates. As the water content increases, the fluorescence intensities of fluoranthene dyes exhibit significant fluorescence quenching with the quenching efficiency as high as 96.5% along with a small red shift in the emission maxima. Significantly, the practical test measurements for the methanol solvent demonstrate the potential of these fluoranthene dyes as probes in the practical application in the measure of the water content in methanol.

Results and discussion

Absorption and fluorescence spectra

The UV-vis absorption and fluorescence spectra of compounds **4a**, **4b** and **4c** were measured in various solvents with different polarities, and the spectral data are presented in Table 1. Compounds **4a** and **4b** show similar spectral properties. As shown in Fig. 1, **4a** and **4b** exhibits an intense absorption band at about 334 nm, which are attributed to the π–π* transition of the conjugated backbone.[40] Compounds **4c** exhibits an broad absorption band at about 387 nm, which are attributed to the π–π* transition of the conjugated backbone.

The fluorescence spectra of three fluoranthene dyes in methanol are shown in Fig. 2. Compound **4a** and **4b** exhibit
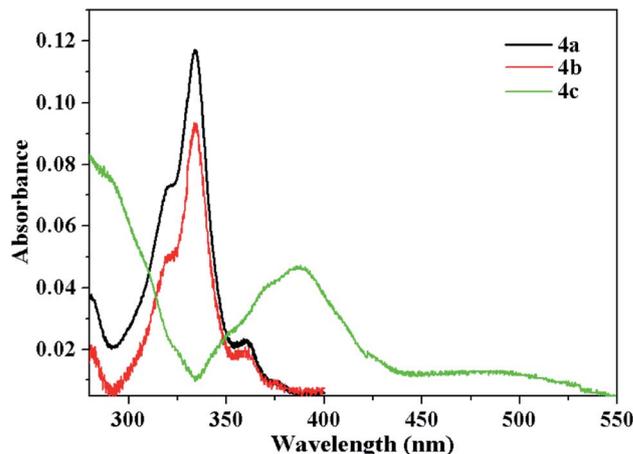

Fig. 1 Absorption spectra of **4a**, **4b** and **4c** in methanol (1×10^{-5} mol L^{-1}).

similar fluorescence spectra with the emission peaks at about 506 nm, while compound **4c** exhibit one emission peak and one shoulder peak at about 473 nm and 537 nm, respectively. Compared to **4a** and **4b**, the maximum emission peaks for **4c** was red-shifted about 34 nm, which is due to the benzo substitutions in edge position. Heinrich's research regarding benzo-fluoranthenes indicates that benzo substitutions at the *b* and *k* position increase Φ_F with a hypsochromic shift in the emission, while *a* and *j* substitutions decrease Φ_F with a bathochromic shift.[44,45]

The fluorescence of compounds **4a–c** in the solid state was measured (Fig. S1†). Comparing to the fluorescence spectra of

Table 1 The spectral characteristics of compounds **4** in different solvents[a]

	Solvent	λ_{abs} (nm)	λ_{em} (nm)	$\Delta\nu$ (cm^{-1})	ε	n	Δf
4a	DMF	337	517	10 331	36.71	1.4305	0.274386
	CH_2Cl_2	335	494	9608	8.93	1.4242	0.217103
	Chloroform	336	491	9395	4.81	1.4459	0.148262
	THF	335	505	10 049	7.58	1.4072	0.209572
	Methanol	334	506	10 177	32.66	1.3284	0.308560
	Ethyl acetate	334	500	9940	6.02	1.3724	0.199635
	n-Hexane	331	479	9334	1.88	1.3749	−0.001364
4b	DMF	337	517	10 331	36.71	1.4305	0.274386
	CH_2Cl_2	335	493	9608	8.93	1.4242	0.217103
	Chloroform	335	490	9395	4.81	1.4459	0.148262
	THF	336	503	10 049	7.58	1.4072	0.209572
	Methanol	334	503	10 059	32.66	1.3284	0.30856
	Ethyl acetate	333	499	9940	6.02	1.3724	0.199635
	n-Hexane	331	478	9334	1.88	1.3749	−0.001364
4c	DMF	390	494	5398	36.71	1.4305	0.274386
	CH_2Cl_2	387	459	4054	8.93	1.4242	0.217103
	Chloroform	388	460	4034	4.81	1.4459	0.148262
	THF	389	479	4831	7.58	1.4072	0.209572
	Methanol	387	473	4662	32.66	1.3284	0.30856
	Ethyl acetate	386	469	4585	6.02	1.3724	0.199635
	n-Hexane	380	445	3844	1.88	1.3749	−0.001364

[a] The excitation wavelength (λ_{ex}), emission wavelength (λ_{em}), Stokes shift ($\Delta\nu$), dielectric constant (ε), refractive index (n), orientation polarizability (Δf).
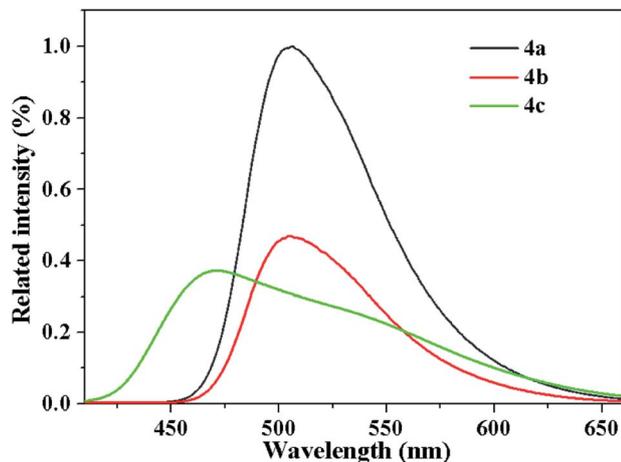
Fig. 2 Emission spectra of **4a**, **4b** and **4c** in methanol (λ_{ex} = 336 nm for **4a** and **4b**, λ_{ex} = 380 nm for **4c**, 1×10^{-5} mol L^{-1}).

these compounds in methanol solution, a red shift of 40–44 nm in the maximum emission peak is observed in the solid.

Effect of solvent polarity

The solvent effect on the fluorescence characteristics of compounds **4a–c** was studied (Fig. 3, S7, S8† and Table 1). As shown in Fig. 3, a gradual red shift in emission peak was observed from 479 nm to 517 nm with the increase of solvent polarity, which indicated that they have more polar in the excited state than in the ground state and increased polarity of the solvent will lower the energy level of the charge transfer excited state.[40]

As summarized in Table 1, the fluorescence spectra of each compound undergo bathochromic shifts with increasing solvent polarity. The effect of solvent polarity can be studied in terms of the difference in the dipole moment between the ground state and the excited states. These were analyzed by a Lippert–Mataga plot, which is essentially a plot of the Stokes
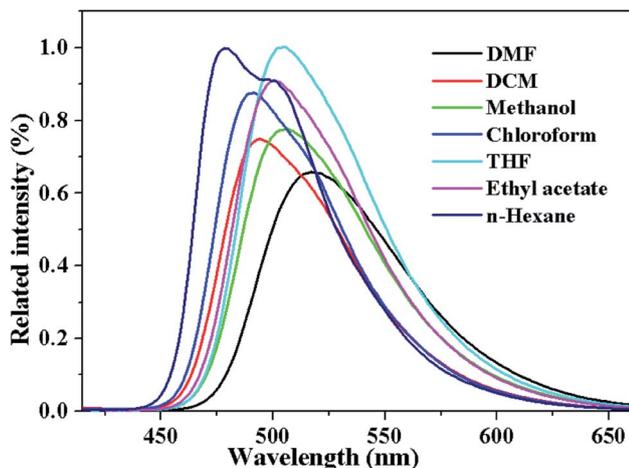
shift of the fluorescence emission *versus* the solvent polarity.[46] The equation is expressed as followed:

$$\Delta \bar{v} = \bar{v}_a - \bar{v}_f = \frac{2}{hc}\left(\frac{\varepsilon - 1}{2\varepsilon + 1} - \frac{n^2 - 1}{2n^2 + 1}\right)\frac{(u^* - u)^2}{a^3} + C$$

$$\Delta f = \frac{\varepsilon - 1}{2\varepsilon + 1} - \frac{n^2 - 1}{2n^2 + 1}$$

where $\Delta \bar{v}$ is Stokes shift, $\bar{v}_a$ and $\bar{v}_f$ are wave numbers of the absorption and emission, respectively. h being Planck's constant and C is the velocity of light in vacuum, e is the solvent dielectric constant, n is the index of refraction, a is the radius residence cavity, μ^* and μ are excited and ground state dipole moment, respectively. Δf accounts for the spectral shifts due to reorientation of the solvent molecules, called the orientation polarizability. In general, the reorientation of the solvent molecules is expected to result in substantial Stokes shifts. As shown in Fig. 4, the Stokes shifts increase with the solvent polarity for the compound **4**. Nevertheless, the poor linearity was found for the overall regression (correlation coefficient is 0.7488), which is because the Lippert–Mataga equation can only partially explain the effect of solvent polarity. The actual deviations of Stokes shifts in seven solvents from the correlations may be due to the effect of the formation of hydrogen bonding. Such hydrogen bond donor-solvents can easily form hydrogen bonds, binding to the carbonylic oxygens of the compound **4**.

Spectral changes induced by addition of water in methanol

The fluorescence emission spectra of **4a** in methanol solution are shown in Fig. 5. The concentration of the indicators was selected at a sufficiently low level (10^{-5} M range) in order to prevent self-quenching effects. As shown in Fig. 5, the fluorescence intensity decreased sharply with the increase in the amount of the water. When the concentration range of water reached 75% (v/v), the emission intensity was almost completely quenched at the high quenching efficiency of 96.5%. The spectra exhibit significant fluorescence quenching with a small red shift in the emission maxima as the water content increases.
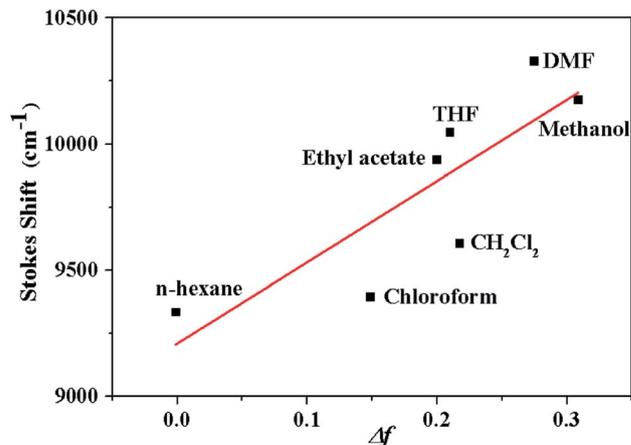

Fig. 3 The emission spectra of compound **4a** in different solvents (λ_{ex} = 336 nm, 1×10^{-5} mol L^{-1}).

Fig. 4 Dependence of the Stokes shift $\Delta \bar{v}$ of **4a** on the solvent polarity function Δf.
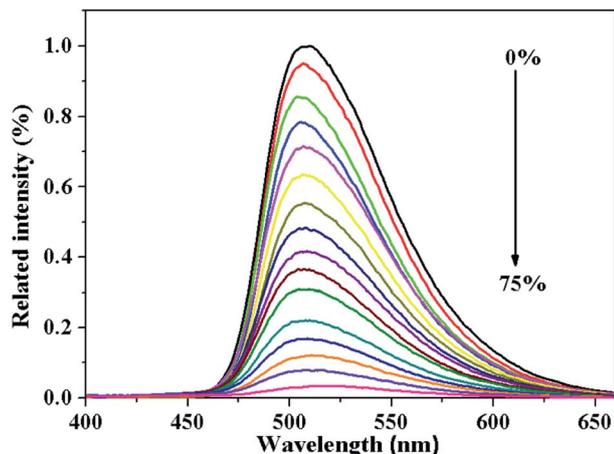
Fig. 5 Fluorescence emission spectra of the **4a** probe contacted with different water contents in methanol in the range of 0 to 75% (v/v, λ_{ex} = 336 nm).

The spectral effects observed for **4b**, **4c** are very similar to the ones of **4a** (Fig. S2 and S3†).

The fluorescence emission spectra of **4a** in other solution, such as ethanol, propanol, CH_3CN and THF, are fulfilled. In addition, the fluorescence spectrum for detecting the water content in ethanol, acetonitrile and THF were fulfilled (Fig. S4†). The quenching efficiency in ethanol, isopropanol and acetonitrile is 81%, 80% and 72%, respectively, which are slightly lower than in methanol. There is almost no quenching of fluorescence in THF.

Quantification using Stern–Volmer equation

The fluorescence quenching efficiency can be quantitatively explained by the Stern–Volmer (SV) equation: $(F_0/F) = 1 + K_{sv}[Q]$, where K_{sv} is the quenching constant, [Q] is the quencher concentration and F_0 and F are fluorescence intensities before and after the addition of the water.[39] The Stern–Volmer curves of the water are almost linear at low concentrations, and subsequently deviated from linearity, bending upwards at higher concentrations. The K_{sv} values of **4a–c** were calculated to be 50.6 for water (Fig. 6, S5 and S6†). The positive curvature from linearity suggests that quenching is not only due to collisions, but also is related to the role of a static quenching process, which has been discussed using the ground state complex or the sphere of action static quenching models.[47] Since the absorption spectra of **4a** in all of the seven solvents show no observable differences in shape or maxima in both the absence and presence of water, the sphere of action static quenching model was used.

Molecular orbital energies

The electronic configurations were further examined using the theoretical models implanted in the Gaussian 09 program.[48] The calculations based upon density functional theory (DFT) (B3LYP; 6-31G) were carried out to obtain the information about the HOMO and LUMO distributions of the compounds **4a–c** in the ground state. All of these compounds possess a high HOMO energy level (−5.52 to −5.75 eV), which could lead to their better hole–transport properties (Fig. 7). For fluoranthene and **4c**, it can be found that both HOMO and LUMO are fully delocalized over the entire molecular system. The HOMO orbital of **4a** and **4b** was slightly altered and LUMO is delocalized on the fluoranthene core. The low LUMO energy of these compounds (−2.24 to −2.56 eV) is supposed to facilitate the acceptance of electrons from the cathode. It is generally indicative of a HOMO/LUMO absorption transition to bear a significant charge-transfer character.

Practical application

The relationship between the fluorescence intensity of three fluorescent probes and the water content in methanol was measured, and the result of plotting the change curve is shown in Fig. 8.
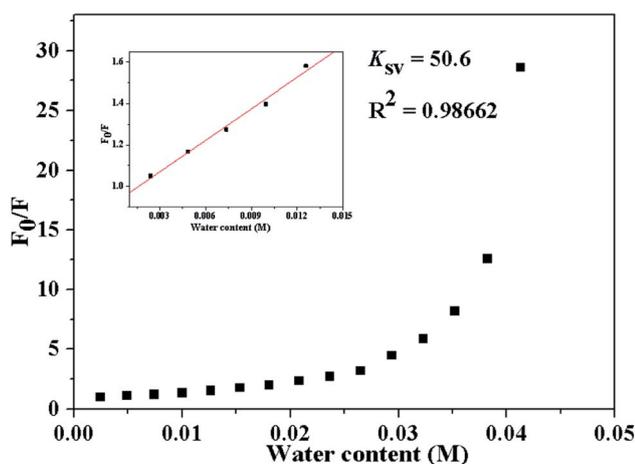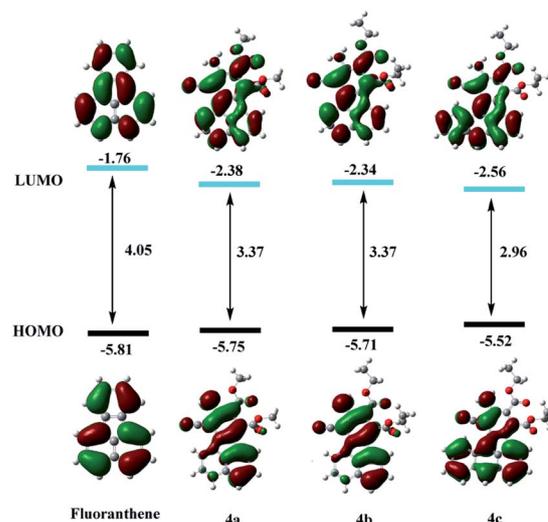

Fig. 6 The Stern–Volmer plots for **4a** in methanol with a low-level of water. The solid lines represent fits to the concentration-resolved data using Stern–Volmer equation.

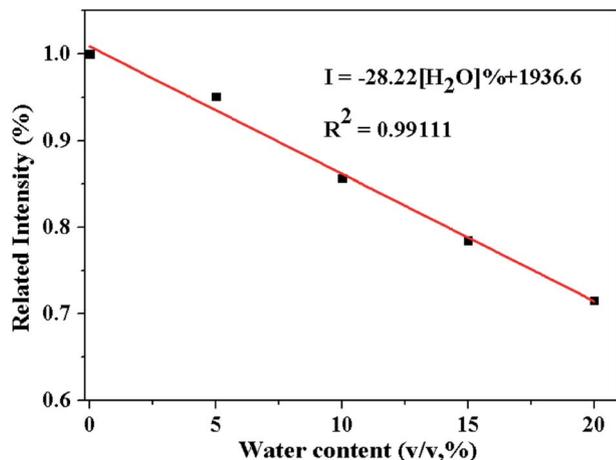**Fig. 7** Calculated molecular orbitals and energy levels of fluoranthene and **4a–c**.

Fig. 8 The linear relationship with water content in methanol for **4a**.

Table 2 Determination of water content in methanol

	$[H_2O]^a$	$[H_2O]^b$b	Relative error %
4a	0.04	0.05	25
	0.06	0.08	33.3
	0.14	0.13	7.1
4b	0.08	0.08	0
	0.12	0.11	8.3
	0.18	0.19	5.6
4c	0.06	0.07	16.7
	0.08	0.10	25
	0.12	0.11	8.3

[a] Water content artificially added in anhydrous methanol (v/v). [b] Water content detected by three probes.

As shown in Fig. 8, when the water content ranges of in methanol was 0–20%, a good linear relationship of the fluorescence intensity of the **4a** and water content ranges of in methanol was provided. The true water content in the solution can be obtained from the linear equation ($I = -28.22C + 1936.6$ $R^2 = 0.99111$). The detection limits was calculated according to the formula reported in the literature.[49,50] Use the above linear equation to determine the methanol water content to test the practical application of these three probes.

As shown in the Table 2, the measurement results of the three fluorescent probes are basically the same as the artificially added water content. These three fluoranthene probes can actually measure the water content in methanol.

Conclusions

In summary, we designed and prepared three new types of fluoranthene fluorescent molecular probes **4a**, **4b** and **4c** by cycloaddition reactions using acrylonitrile and dialkyl acetylenedicarboxylates. Their fluorescence properties in different polar–organic solvents were investigated systematically. Water shows a significant quenching effect, and consequently these fluoranthenes dyes can be efficiently used to detect the water

content in methanol as probes. Significantly, the practical test measurements for the water contents in methanol that the deviation between the actual result and the measured result is within a relatively small range, providing a potential of these fluoranthene dyes as probes in the practical application in the measure of the water content in methanol.

Experimental section

Chemicals and instruments

All reactants were commercially available and used without further purification. Melting points were recorded on electro-thermal digital melting point apparatus and were uncorrected. ^{1}H and ^{13}C NMR spectra were recorded at 295 K on a Varian INOVA 400 MHz or a Varian NMR System 300 MHz spectrometer using CDCl$_3$ or d_6-DMSO as solvent and TMS as internal standard. UV-vis spectra were recorded on a Shimadzu UV-2501PC spectrometer; fluorescence spectra were obtained on an Hitachi FL-4600 spectrofluorimeter; HRMS data were measured using TOF-MS(EI+) instrument. The synthetic routines are shown in Scheme 1.

General procedure for the preparation of compounds 4

To a magnetically stirred solution of 2-(2-oxoaceanthrylen-1(2H)-ylidene)malononitrile (**1a**, 1 mmol), the corresponding dialkyl acetylenedicarboxylate (**2**, 1 mmol) and DBU (1 mmol) in toluene and water (v_t/v_w = 100 : 1, 2.0 mL) was added dropwise to a solution of corresponding isocyanide (**3**, 1 mmol) in toluene and water (v_t/v_w = 100 : 1, 1.0 mL) at 25 °C for 5 min. The reaction mixture was then stirred at 130 °C for 24 h. The solvent was removed and the residue was purified by column chromatography using n-hexane–EtOAc (1 : 5) as eluent. The solvent was removed and the product was obtained. The structures of compounds **4** were deduced from their IR, ^{1}H NMR, ^{13}C NMR, and high-resolution mass spectrometry (HRMS) spectra.
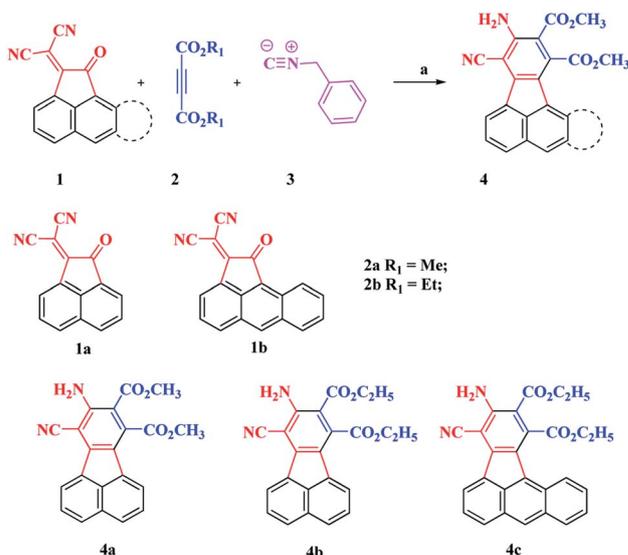
Scheme 1 The synthetic routines for fluoranthene dyes **4**. Reagents and conditions: (a) Toluene, H$_2$O, DBU, 130 °C.

Dimethyl 9-amino-10-cyanofluoranthene-7,8-dicarboxylate (4a). Mp 198–201 °C, yellow powder, yield 40%, IR(KBr): 3339, 2948, 2212, 1730, 1697, 1604, 1556, 1436, 1250, 1094, 768 cm^{-1}, ^{1}H NMR (400 MHz, CDCl$_3$) δ 8.37 (d, J = 7.1 Hz, 1H), 7.90 (d, J = 8.2 Hz, 1H), 7.76 (d, J = 7.9 Hz, 1H), 7.65–7.52 (m, 3H), 6.71 (s, 2H), 4.08 (s, 3H), 3.92 (s, 3H), ^{13}C NMR (101 MHz, CDCl$_3$) δ 168.4, 166.6, 151.5, 146.3, 134.5, 133.4, 132.7, 132.0, 130.1, 129.7, 128.3, 127.9, 126.6, 124.9, 124.1, 121.2, 115.6, 106.3, 92.7, 52.8, 52.6; HRMS(ESI) calcd for C$_{21}$H$_{14}$N$_2$O$_4$ [M − H]$^-$ 357.0875, found 357.0876.

Diethyl 9-amino-10-cyanofluoranthene-7,8-dicarboxylate (4b). Mp 187–190 °C, yellow powder, yield 42%, IR(KBr): 3429, 2962, 2220, 1734, 1689, 1607, 1553, 1427, 1312, 1194, 1050, 767 cm^{-1}, ^{1}H NMR (400 MHz, CDCl$_3$) δ 8.43 (d, J = 7.1 Hz, 1H), 7.94 (d, J = 8.2 Hz, 1H), 7.80 (d, J = 8.2 Hz, 1H), 7.64 (m, 3H), 6.77 (d, J = 5.0 Hz, 2H), 4.57 (m, 2H), 4.41 (m, 2H), 1.44 (m, 6H). ^{13}C NMR (101 MHz, CDCl$_3$) δ 167.9, 166.4, 151.6, 146.2, 135.0, 133.4, 133.0, 132.1, 130.1, 129.8, 128.4, 128.0, 126.5, 124.9, 124.1, 121.3, 115.7, 106.6, 92.6, 62.0, 61.8, 14.1, 14.1; HRMS(ESI) calcd for C$_{23}$H$_{18}$N$_2$O$_4$ [M−H]$^-$ 385.1188, found 385.1187.

Diethyl 2-amino-1-cyanobenzo[a]aceanthrylene-3,4-dicarboxylate (4c). Mp 210–213 °C, red powder, IR (KBr): 2954, 2227, 1731, 1686, 1574, 1439, 1364, 1299, 1052, 776 cm^{-1}; ^{1}H NMR (400 MHz, CDCl$_3$) δ 8.55 (d, J = 8.0 Hz, 1H), 8.42 (s, 1H), 8.15 (d, J = 8.0 Hz, 1H), 8.11–8.03 (m, 2H), 7.64 (m, 1H), 7.55–7.43 (m, 2H), 6.19 (s, 2H), 4.45 (m, 4H), 1.41 (t, J = 8.0 Hz, 3H), 1.17 (t, J = 8.0 Hz, 3H); ^{13}C NMR (100 MHz, CDCl$_3$) δ 169.7, 167.1, 148.9, 145.2, 134.8, 132.2, 130.6, 130.5, 129.5, 128.7, 128.2, 127.2, 127.1, 126.9, 125.3, 125.0, 124.8, 115.9, 110.5, 92.6, 62.1, 61.9, 31.9, 22.7, 14.0, 13.6; HRMS (APCI) calcd for C$_{27}$H$_{20}$N$_2$O$_4$ [M−H]$^-$ 435.1345, found 435.1342.

X-ray crystallography

Unambiguous evidence for the structure of **4a** was obtained from single-crystal X-ray analysis. The structure diagram of
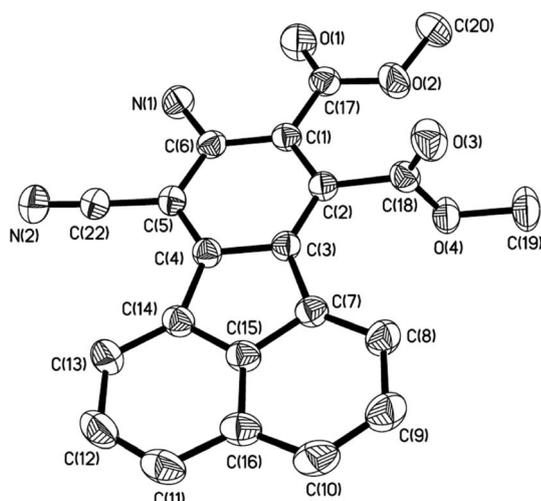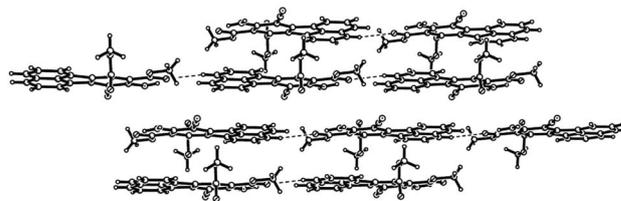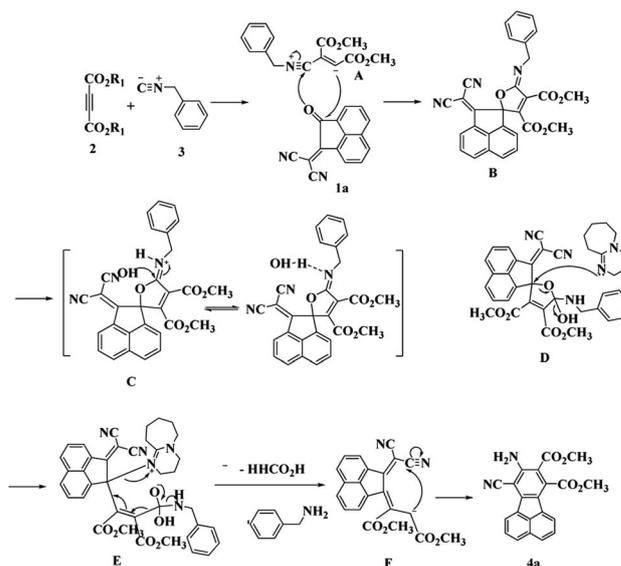

Fig. 10 The crystal packing of **4a** with the dashed lines represent the hydrogen bonding interactions.

Scheme 2 Plausible mechanistic pathway.

these compounds **4a** was shown in Fig. 9. (CCDC reference numbers 2093383). Compound **4a** crystallizes in a triclinic lattice with the space group in the $P\bar{1}$ space group (Table S1†). The molecule of **4a** is nearly planar and the largest deviation from the least-squares plane through all the atoms is 0.0419 (4) Å for C2.

The crystal packing shows that the molecules **4a** are linked *via* C–H···O (C10–H10···O1 3.414 Å) and N–H···O (N1–H2···O5 2.915 Å) hydrogen bonds to form layers, and the adjacent layers are further connected *via* C–H···N (C20–H20c···N2 3.645 Å, C19–H19b···N2 3.316 Å) hydrogen bonds and π–π interactions (Fig. 10). The π–π distances are about 3.9 Å for **4a** (dependent on the point of measurement). The final 3D crystal packing is further stabilized by van der Waals forces.

Based on the experimental results and our previous research reports,[40] a possible mechanism for the reaction is proposed in Scheme 2. The initial event is formation of the spiro-substitute furan B. Subsequently, in the presence of H$_2$O and DBU, product B undergoes a rearrangement to yield fluoranthene **4**.

Conflicts of interest

There are no conflicts to declare.

Fig. 9 Ortep diagram of **4a**, displacement ellipsoids are shown with 40% probability.

Notes and references

1 P. Kumar, A. Ghosh and D. A. Jose, *ChemistrySelect*, 2021, **6**, 820–842.

2 T. I. Kim and Y. Kim, *Anal. Chem.*, 2017, **89**, 3768–3772.

3 A. Cedergren and C. Oraedd, *Anal. Chem.*, 1994, **66**, 2010–2016.

4 I. Nordin-Andersson and A. Cedergren, *Anal. Chem.*, 1985, **57**, 2571–2575.

5 C. Oraedd and A. Cedergren, *Anal. Chem.*, 1994, **66**, 2603–2607.

6 C. Oraedd and A. Cedergren, *Anal. Chem.*, 1995, **67**, 999–1004.

7 R. Oguchi, K. Yamaguchi and T. Shibamoto, *J. Chromatogr. Sci.*, 1988, **26**, 588–590.

8 J. P. Schmit and G. Boulay, *Anal. Chem.*, 1981, **53**, 2359–2361.

9 G. Casalbore-Miceli, Y. S. Chen, E. M. Girotto, Y. Li, A. W. Rinaldi, M. J. Yang and A. Zanelli, *Sens. Actuators, B*, 2006, **119**, 577–582.

10 G. Casalbore-Miceli, A. Zanelli, A. W. Rinaldi, E. M. Girotto, M. J. Yang, Y. S. Chen and Y. Li, *Langmuir*, 2005, **21**, 9704–9708.

11 H. Huang and P. K. Dasgupta, *Anal. Chem.*, 1990, **62**, 1935–1942.

12 S. Cho, H. Chung, Y. A. Woo and H. J. Kim, *Bull. Korean Chem. Soc.*, 2005, **26**, 115–118.

13 C. G. Niu, P. Z. Qin, G. M. Zeng, X. Q. Gui and A. L. Guan, *Anal. Bioanal. Chem.*, 2007, **387**, 1067–1074.

14 Y. Sun, X. Liang, S. Wei, J. Fan and X. Yang, *Spectrochim. Acta, Part A*, 2012, **97**, 352–358.

15 C. Niu, L. Li and P. Qin, *Anal. Sci.*, 2010, **26**, 671–674.

16 W. Liu, Y. Wang, W. Jin, G. Shen and R. Yu, *Anal. Chim. Acta*, 1999, **383**, 299–307.

17 J. S. Kim, M. G. Choi, Y. Huh, S. H. Kim and S. K. Chang, *Bull. Korean Chem. Soc.*, 2006, **27**, 2058–2060.

18 J. Maillard, K. Klehs, C. Rumble, E. Vauthey, M. Heilemann and A. Furstenberg, *Chem. Sci.*, 2020, **12**, 1352–1362.

19 R. S. Kumar, J. Jeong, N. Mergu, W. Oh and Y.-A. Son, *Dyes Pigm.*, 2017, **136**, 458–466.

20 H. Wang, Y. Li, S. Yang, H. Tian, S. Liang and B. Sun, *ACS Omega*, 2019, **4**, 10695–10701.

21 Q. Chang, Z. Murtaza, J. R. Lakowicz and G. Rao, *Anal. Chim. Acta*, 1997, **350**, 97–104.

22 K. N. Kim, K. C. Song, J. H. Noh and S. K. Chang, *Bull. Korean Chem. Soc.*, 2009, **30**, 197–200.

23 Y. Ooyama, H. Egawa and K. Yoshida, *Eur. J. Org. Chem.*, 2008, **2008**, 5239–5243.

24 Y. Ooyama, H. Egawa and K. Yoshida, *Eur. J. Org. Chem.*, 2010, **2008**, 5239–5243.

25 L. Ding, H.-Z. Ying, Y. Zhou, T. Lei and J. Pei, *Org. Lett.*, 2010, **12**, 5522–5525.

26 X.-L. Fang, S.-L. Deng, J. Wang, X.-F. Wang, C. Chen, Y. Li, S.-Y. Xie, R.-B. Huang and L.-S. Zheng, *Chem. Mater.*, 2009, **21**, 5763–5771.

27 A. Goel, V. Kumar, S. Chaurasia, M. Rawat, R. Prasad and R. S. Anand, *J. Org. Chem.*, 2010, **75**, 3656–3662.

28 A. Goel, A. Sharma, M. Kathuria, A. Bhattacharjee, A. Verma, P. R. Mishra, A. Nazir and K. Mitra, *Org. Lett.*, 2014, **16**, 756–759.

29 C. Kazunga, M. D. Aitken, A. Gold and R. Sangaiah, *Environ. Sci. Technol.*, 2001, **35**, 917–922.

30 A. Sygula, S. D. Karlen, R. Sygula and P. W. Rabideau, *Org. Lett.*, 2002, **4**, 3135–3137.

31 S. Kumar, D. Kumar, Y. Patil and S. Patil, *J. Mater. Chem. C*, 2016, **4**, 193–200.

32 S. Kumar, N. Venkatramaiah and S. Patil, *J. Phys. Chem. C*, 2013, **117**, 7236–7245.

33 A. Sharma, A. K. Jha, S. Mishra, A. Jain, B. S. Chauhan, M. Kathuria, K. S. Rawat, N. M. Gupta, R. Tripathi, K. Mitra, M. Sachdev, M. L. B. Bhatt and A. Goel, *Bioconjugate Chem.*, 2018, **29**, 3606–3613.

34 X. Sun, F. Wu, C. Zhong, L. Zhu and Z. Li, *Chem. Sci.*, 2019, **10**, 6899–6907.

35 P. Rietsch, M. Zeyat, O. Hubner, K. Hoffmann, M. Kutter, A. Paskin, J. Uhlig, D. Lentz, U. Resch-Genger and S. Eigler, *J. Phys. Chem. B*, 2021, **125**, 1207–1213.

36 A. T. A. Boraei, H. A. Ghabbour, A. A. M. Sarhan and A. Barakat, *ACS Omega*, 2020, **5**, 5436–5442.

37 X. Chen, L. Zhang, Y. Wang, G. Qiu, Q. Liang and H. Zhou, *J. Org. Chem.*, 2020, **85**, 12526–12534.

38 D. Khiri, D. Q. Dao, B. T. Nguyen, L. Gasnot, F. Louis and A. El Bakali, *J. Phys. Chem. A*, 2019, **123**, 7491–7498.

39 R. Guo, H. Dong, P. Li, Y. Sun, H. Wang and H. Liu, *CrystEngComm*, 2020, **22**, 5882–5889.

40 H.-Y. Liu, L.-F. Chen, H.-Y. Wang, Y. Wan and H. Wu, *RSC Adv.*, 2016, **6**, 94833–94839.

41 H.-Y. Liu, G.-M. Gao, J. Liu and H.-Y. Wang, *Polyhedron*, 2018, **152**, 11–16.

42 H.-Y. Wang, J.-J. Shi, C. Wang, X.-X. Zhang, Y. Wan and H. Wu, *Dyes Pigm.*, 2012, **95**, 268–274.

43 H. Liu, G. Gao, J. Liu, F. Bao, Y. Wei and H. Wang, *CrystEngComm*, 2019, **21**, 2576–2584.

44 G. S. Mohammad-Pour, R. T. Ly, D. C. Fairchild, A. Burnstine-Townley, D. A. Vazquez-Molina, K. D. Trieu, A. D. Campiglia, J. K. Harper and F. J. Uribe-Romo, *J. Org. Chem.*, 2018, **83**, 8036–8053.

45 G. Saranya, P. Kolandaivel and K. Senthilkumar, *J. Phys. Chem. A*, 2011, **115**, 14647–14656.

46 H. Park and S.-K. Chang, *Dyes Pigm.*, 2015, **122**, 324–330.

47 Z. Li, Q. Yang, R. Chang, G. Ma, M. Chen and W. Zhang, *Dyes Pigm.*, 2011, **88**, 307–314.

48 M. J. Frisch, G. W. Trucks, H. B. Schlegel, G. E. Scuseria and M. A. Robb, *Gaussian 09*, Gaussian Inc., Wallingford CT, 2009.

49 L. Peng, Q. Zhao, D. Wang, J. Zhai, P. Wang, S. Pang and T. Xie, *Sens. Actuators, B*, 2009, **136**, 80–85.

50 P. Wu, Y. Liu, Y. Liu, J. Wang, Y. Li, W. Liu and J. Wang, *Inorg. Chem.*, 2015, **54**, 11046–11048.